ACS APPLIED MATERIALS & INTERFACES

Research Article

www.acsami.org

Zwitterionic-Based Stainless Steel with Well-Defined Polysulfobetaine Brushes for General Bioadhesive Control

Mei-Chan Sin,[†,‡] Yi-Ming Sun,*[,†,‡,§] and Yung Chang*[,†]

[†]R&D Center for Membrane Technology and Department of Chemical Engineering, Chung Yuan Christian University, Chung-Li, Taoyuan 320, Taiwan

[‡]Department of Chemical Engineering and Materials Science and [§]Graduate School of Biotechnology and Bioengineering, Yuan Ze University, Chung-Li, Taoyuan 320, Taiwan

Supporting Information

ABSTRACT: Stainless steels are widely used as orthopaedic and dental implant; however, bioadhesion in the case of thrombosis, inflammation, and infection is one of their major limitations. One way to tackle this problem is to graft the stainless steel surface with a zwitterionic polymer known for being anti-bioadhesive. Controlled atom transfer radical polymerization (ATRP) of zwitterionic poly(sulfobetaine methacrylate) (polySBMA) grafted from biomedical grade stainless steel surface was employed in this study. The interactions of polySBMA-grafted surfaces with biomacromolecules were demonstrated in vitro by the adhesion tests of plasma protein, blood cells, human MG63 osteoblast- and HT1080 fibroblast-like cells in biological complex media to evaluate their bioadhesive properties. Anti-microbial effects were also assessed for two most ordinary seen clinical bacteria, i.e., *Escherichia coli* and *Staphylococcus epidermidis*. Results showed that polySBMA-grafted surface exhibited evident bioadhesion resistance and conferring antibacterial efficacy. This work is also dedicated to deduce the effectiveness of polySBMA brushes' conformational structure on the prevention of bioadhesion. To this aim, the anti-bioadhesive effect of polySBMA brushes prepared by dopamine- and silane-surfaced immobilization method was evaluated. Results show that polySBMA grafted from immobilized polydopamine interfacial layers achieved better bioadhesion resistance, which could be causally related to their greater grafting coverage, flexible brush conformational structures, and greater hydration capabilities.

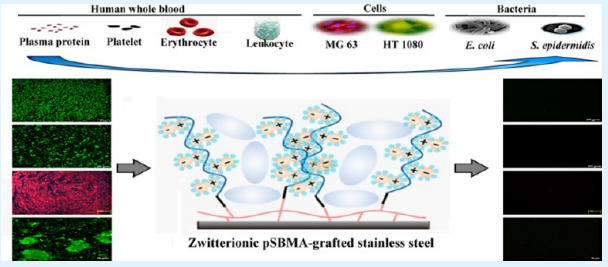

KEYWORDS: *stainless steel, zwitterionic polysulfobetaine, polydopamine, anti-bioadhesion, polymer brushes*

INTRODUCTION

For more than 100 years, metallic biomaterials have been exploited as biomedical implants, since Lane first introduced metal plate[1] for bone fracture fixation in 1895. Stainless steels (SUS) are widely used as surgical implants in orthopaedic and dental applications, e.g., coronary and pulmonary stents, hip prosthesis, screws, fixations, etc., because of the good mechanical properties, chemical stability, resistance to general corrosion, bio-inertness, and biocompatibility.[2,3] The excellent biocompatibility of stainless steel is reportedly attributable to the stable oxide that readily forms on its metal surfaces.[3,4] Nevertheless, stainless steel–based surgical implantation is still correlated with some clinical problems. The reaction of implanted foreign biomaterial with human body is usually very complex. When the implanted metal is brought into contact with physiological fluid, a series of protein adsorption, platelet adhesion, complement and leukocyte activation are provoked by the human defense system. This will ultimately lead to unfavorable foreign-body response, leading to thrombosis and failure of the biomaterials.[5−8] Furthermore, upon recovery, SUS implants need to be removed from the patient's body. Thus, it is critical to reduce bone cells or interfacial fibrous tissue attachment to the implant surface in order to avoid subsequent second damage to the healed bone and adjacent soft tissues.

The infection risk of biomaterial implants is another major clinical problem[9] that could result in implant failure, and subsequently serious intricacies with high morbidity and surgery costs. On the basis of the previous studies of implant-related infections, these complications may arise from the circulation of bacteria in the bloodstream to the implant or bacteria from patient's own skin and/or mucosa entering the wound site during implant surgical insertion.[10−13] Bacterial adhesion and subsequent growth results in slime enclosed biofilm formation on the implant surface, which act as a barrier to against the host defence mechanisms or antibiotics. Studies have been shown that both specific antibacterial antibodies and activated leukocytes were ineffective in killing these slime protected biofilm bacteria.[14,15] Besides that, Khoury et. al. (1992) indicate that 500−5000 times higher levels of antibiotics are needed to achieve the same antimicrobial effects on biofilm bacteria than needed for free-floating bacteria.[16]

Received: September 22, 2013
Accepted: December 18, 2013
Published: December 18, 2013

Scheme 1. Schematic Illustration of the Preparation Process of Zwitterionic PolySBMA Grafting from Stainless Steel via ATRP Using (a) Catechol Dopamine and (b) Organosilane As Respective Self-Assembly Anchoring Agent

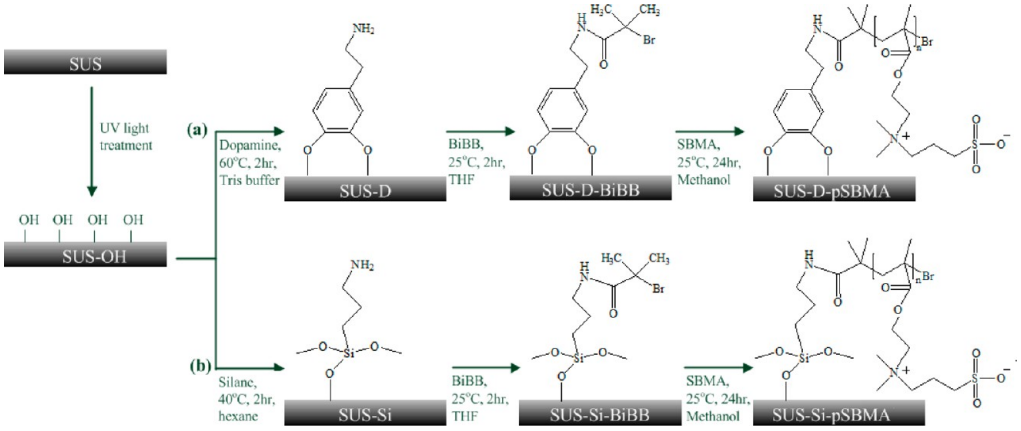

Therefore, the initial adhesion of bacteria to biomaterial surfaces is believed to be critical in the pathogenesis of infection.[13,17]

It is generally believed that reducing bioadhesion could significantly attenuate subsequent adverse inflammatory responses including thrombosis coagulation, leukocyte activation, tissue inflammation and bacterial infection. The ability to reduce the incidence of thrombosis, inflammation and implant-associated infections is essentially crucial for the design of biocompatible SUS surface.[18,19] Surface modification is a method applicable to implant technology because it can enhance the biocompatibility of SUS surface by providing specific anti-bioadhesive properties on the metallic surface through proper molecular design while keeping the bulk properties intact.[20] Surface-initiated atom transfer radical polymerization (SI-ATRP) is well-suited for anti-bioadhesive polymerization on biomaterial surfaces since the method can offer versatility in selection of monomers, mild reaction conditions, aqueous or methanolic media, and the possibility to obtain well-defined polymer structures.[21−23]

Modification of SUS surface with grafting of nonfouling zwitterionic polymer films via ATRP could limit the interactions between the metal and physiological fluids, tissues and microorganisms. Zwitterionic polymers have gained increasing importance for the employment as bio-inert surfaces due to their outstanding suppression in plasma protein adhesion, blood platelet adsorption and activation, and thrombus formation in vitro.[24−28] A general characteristic of zwitterionic materials, including phosphobetaine, sulfobetaine or carboxylbetaine, is that they have both positive and negative charged moieties on the same side chain, maintaining total charge neutrality.[29−32] Recently, zwitterionic poly(sulfobetaine methacrylate) (polySBMA) has been extensively explored because of its ease of synthesis and applicability[30,33] and it could exhibit greater stability in complex media or in vivo when compared to poly(ethylene glycol), which may be decomposed in the presence of oxygen and transition metal ions when in contact with biochemically relevant solutions for a long period.[34,35] Besides that, polySBMA polymers were found to be non-cytotoxic and their endotoxin levels were found to be acceptable for in vivo implantation according to Zhang et. al (2009).[36] It was claimed that the bio-inert nature of zwitterionic polySBMA polymers is attributed to their strong hydration capabilities and the tightly bound, structured water layer around the zwitterionic pendant groups through electrostatically induced hydration, which play an important part in affording interfacial bioadhesion resistance.[31,33,37]

In this study, a catalog of surface modification to the biomedical grade 316L type stainless steel (SUS 316L) was adopted in an effort to govern the feature of host reactions in terms of thrombosis, inflammation and bacterial infection. We demonstrated the use of respective biomimetic catecholic and organosilane initiator for SI-ATRP from SUS 316L surfaces to graft anti-bioadhesive polySBMA brushes. Catecholic dopamine and organosilane were served as the respective anchor site for subsequent immobilization of ATRP initiator and polySBMA polymerization. PolySBMA brushes grown from the respective dopamine and silane-assembly layers were compared for the effectiveness in resisting the adhesion of plasma protein, blood cells, mammalian cells, and bacteria.

MATERIALS AND METHODS

Materials. 316L type stainless steel coupons (SUS 316L) used in this study was purchased from Walsin Lihwa Corporation (Taiwan) (5 mm in diameter, 1 mm in thickness). [2-(Methacryloyloxy)ethyl]-dimethyl(3-sulfopropyl)-ammonium hydroxide (sulfobetaine methacrylate, SBMA) macromonomer was purchased from Monomer-Polymer & Dajac Laboratories, Inc. in the United States. Copper(I) bromide (99.999%), 2-bromoisobutyryl bromide (BiBB, 98%), pyridine (98%), 2,2′-bipyridine (BPY, 99%), triethylamine (99%), tetrahydrofuran (THF, HPLC grade), dopamine hydrochloride ($C_8H_{11}NO_2HCl$), 3-aminopropyl trimethoxysilane (95%) and ethanol (absolute 200 proof) were purchased from Sigma-Aldrich. Fibrinogen (fraction I from human plasma) was purchased from Sigma Chemical Co. Deionized water used in the experiments was purified using a Millipore water purification system with a minimum resistivity of 18.0 MΩ m. THF used for reactions was dried by calcium hydride before use. Nitrogen gas was of high purity grade.

Preparation of Surface Grafted PolySBMA Brushes via ATRP. A schematic illustration of the synthesis of zwitterionic polySBMA brushes grafted from stainless steel via ATRP method is shown in Scheme 1. Prior to surface modification, SUS 316L coupons were washed with absolute ethanol for 10 min by sonication. Cleaned stainless steel coupons were left in an ultraviolet irradiation chamber for 20 min at a source power of 110 W followed by cleansing with ethanol and deionized water. For dopamine as anchoring agent, SUS coupons were immersed in an aqueous dopamine solution (1 mg/mL dopamine hydrochloric, in pH 8.5 Tris buffer) at 60 °C for 2 h, followed by cleansing with ethanol and deionized water to remove unbound dopamine. For organosilane as anchoring agent, SUS coupons were immersed in an organosilane solution (200 μL 3-aminopropyl trimethoxysilane in 20 mL hexane) at 40 °C for 2 h,

dx.doi.org/10.1021/am4041256 | ACS Appl. Mater. Interfaces 2014, 6, 861−873

followed by rinsing with ethanol and deionized water for 2 min by sonication to remove unattached self-assembled organosilane.

SUS 316L coupons with amino-terminated self-assembly layers were then reacted with 2-bromoisobutyrl bromide (BIBB) initiator under nitrogen protection with anhydrous operation. In this reaction, reactive SUS coupons were incubated in 15 mL of dry THF with 0.5 mL of triethylamine, and then 0.445 mL of BIBB was added to the solution. A white precipitate, likely pyridine hydrobromide, formed at the initial stage of reaction. After 24 h of reaction at room temperature, the substrates were washed sequentially with THF, acetone, ethanol, and deionized water and were kept in deionized water for subsequent polymerization.

Polymerization of SBMA was taken place in the absence of oxygen. Therefore the following experiment was operated in drybox. Copper(I) bromide and 2,2′-bipyridine were first dissolved in methanol in a sealed glass bottle and transferred to a reactor containing SUS coupons with immobilized initiators, under nitrogen stream. Subsequently a 0.2 M degassed SBMA monomer solution containing 1:3 mixture of deionized water and methanol was added to the reactor under nitrogen flow. The reaction mole ratio for SBMA:CuBr:BPY is 15:1:2. After 24 h of polymerization at room temperature, the substrate was removed and rinsed with ethanol and deionized water.

Freshly cleaned SUS 316L coupon was used as the control in all bioadhesive experiments and was denoted as SUS; dopamine-anchored and silane-anchored stainless steel surface were denoted as SUS-D and SUS-Si, respectively; BiBB immobilized on dopaminized and silanized assembly surface were denoted as SUS-D-BiBB and SUS-Si-BiBB, respectively; and polySBMA brushes grafted from dopaminized and silanized interfacial layers were denoted as SUS-D-pSBMA and SUS-Si-pSBMA, respectively, in the subsequent discussion.

Surface Characterization. The surface compositions of the bare and functionalized SUS surfaces were characterized by X-ray photoelectron spectroscopy (XPS). XPS analysis was performed as described in Chang et. al. (2010),[31] using a PHI Quantera SXM/Auger spectrometer with a monochromated AlKRX-ray source (1486.6 eV photons). The energy of emitted electrons was measured with a hemispherical energy analyzer at pass energies ranging from 50 to 150 eV. All data were collected at the photoelectron take off angle of 45° with respect to the sample surface. The binding energy (BE) scale was referenced by setting the peak maximum in the C 1s spectrum to 284.6 eV. The high-resolution N 1s, C 1s, Br 3d, and S 2p spectrum was fitted using a Shirley background subtraction and a series of Gaussian peaks. Data analysis software was purchased from Service Physics, Inc. The thickness of the respective polydopamine layer, silane monolayer and polySBMA films formed from respective substrate was measured using spectroscopic ellipsometry (HORIBA Jobin Yvon, France). Five various spots of the substrate were evaluated at 70° incident angle in the visible region. Stainless steel substrate was cleaned by UV light treatment for 20 min, washed with ethanol and deionized water, dried with nitrogen gas, and subsequently used as the reference. The surface morphology and topology of pristine and functionalized SUS substrates were observed using tapping-mode atomic force microscopy (TM-AFM) in dry state. In TM-AFM measurement, a commercial Si cantilever (TESP tip) of about 150 kHz resonant frequencies from JPK was used. Static water contact angles of bare and functionalized SUS surfaces were measured with an automatic contact angle-meter (Model CA-VP, Kyowa Interface Science Co., Ltd., Japan). Four microliters of deionized water was dripped on the substrate surface at five various spots. Mean values of water contact angle were then taken.

Plasma Protein Adsorption. The fibrinogen adsorption of human plasma solution onto various surface-modified stainless steel was measured using enzyme-linked immunosorbent assay (ELISA) based on the standard protocol as depicted previously.[37,38]

Human Blood-Platelet Adhesion and Activation. Blood was acquired from a healthy human volunteer. Platelet rich plasma (PRP) containing about 1×10^5 cells/mL was prepared by centrifugation of the blood at 1200 rpm for 5 min and then at 3000 rpm for 10 min. The platelet concentration was measured using a microscopy (NIKON TS 100F). 1 mL of the platelet suspension plasma was allocated in each well of TCP on the bare and various functionalized SUS surface and incubated for 120 min at 37 °C. Blood platelets adhered to the substrate surfaces were stained with 3 μL of CD3-FITC, CD14-FTIC, and CD45-FITC in 270 μL of PBS with 2.5% glutaraldehyde at 4 °C for 15 min. After rinsing with PBS thrice, the morphology of adhered platelets on the substrates in PBS was detected using confocal laser scanning microscopy (NIKON CLSM AIR instrument) at a 200× magnification from five various spots on the similar sample. During observation, the images were taken at λ_{ex} = 488 nm/λ_{em} = 520 nm for detection of the FITC dye. The number of attached platelets on the samples was determined by using ImagePro software.

To test the activated platelets adhesion on the substrates, 200 μL of the platelet rich plasma (PRP), first recalcified by the addition of calcium (1M $CaCl_2$, 5 μL), was placed on the substrate surface in each well of the tissue culture plate and incubated for 120 min at 37 °C. After the samples were rinsed twice with 1 mL of PBS, they were immersed in 2.5% glutaraldehyde of PBS for 48 h at 4°C to fix the adhered platelets and adsorbed proteins. Then, they were rinsed twice with 1 mL of PBS and gradient-dried with ethanol in 90% (v/v) PBS, 75% (v/v) PBS, 50% (v/v) PBS, 25% (v/v) PBS, 10% (v/v) PBS, and 0% (v/v) PBS for 5 min in each step and dried in air. Finally, the samples were sputter-coated (Toshiba E-1010 ion sputter) with gold prior to observation under JEOL JSM-5410 SEM operating at 7 keV.

Human Blood Erythrocyte and Leukocyte Adhesion. Fresh whole blood acquired from healthy human volunteers was mixed with 35 mL of citrate phosphate dextrose adenine-1 (CPDA-1). For isolating erythrocytes, erythrocyte cell fractions were prepared by centrifugation at 1200 rpm for 5 min and the cell pellets were sedimented to the bottom. Erythrocytes fraction was then collected from the bottom centrifuged layer. For isolating leukocytes, diluted blood sample was carefully layered on Ficoll-Paque PLUS. Leukocyte cell fractions were centrifuged at 400 × g at 25°C for 40 min, and collected from the interface between the two phases, whereby erythrocytes were sedimented to the bottom and the upper layer consists of plasma supernatant. 1 mL of respective blood erythrocyte and leukocyte solutions was allocated in each well of the TCP on the sample surface and incubated for 120 min at 37 °C. Morphological observations of adhering blood erythrocytes and leukocytes on the sample surface were performed using CLSM and SEM analyses, by preparing the samples according to the protocol as described previously.

Mammalian Cell Culture and Attachment. In this study, human osteoblast MG-63 cells were obtained from Food Industry Research and Development Institute, Hsinchu, Taiwan. The Dulbecco's modified eagle medium (DMEM) (HyClone) supplemented with 10% fetal bovine serum (HyClone), 1% sodium pyruvate (GIBCO), and 1% Antibiotic Antimycotic (GIBCO) was used as the osteoblast culture medium. The cells were incubated in a humidified incubator in the presence of 5% CO_2 at 37°C. For the initial cell tests, the cells were plated at a density of 1.5×10^5 cells/cm^2. After seeding the MG63 cells on the substrates for 24 h, the adherent cells on substrate surfaces were fixed with 3% glutaraldehyde (Sigma), washed with PBS, and then permeabilized with 0.1% Triton X100 (Sigma). Samples were then rinsed with PBS and incubated with DAPI (KPL) and rhodamine phalloidin (Molecular Probe, Invitrogen) to label nuclei and F-actin microfilaments of the cells. Immunofluorescence images of the attached MG63 cells were taken by using fluorescence microscopy (Olympus, IX 71).

Human fibroblasts (HT-1080) cells (ATCC, Manassas, VA) exhibiting bright green fluorescence (containing EGFP gene) were employed in this study. HT-1080 fibroblasts were cultivated in DMEM supplemented with 10% fetal bovine serum, 100 U/mL penicillin, and 100 μg/mL streptomycin, and incubated in a humidified atmosphere of 5% CO_2 at 37 °C. The substrates were placed in a 24-well TCP plate and each substrate was carefully seeded with 1 mL of cell suspension of 6×10^4 cells/mL concentration. The cells were then cultivated with the substrates for 24 h under similar cultivation condition. Cell morphology and proliferation was detected using a Nikon TS100 microscope equipped with a digital camera using a 20× objective lens and a blue excitation fluorescence filter at the excitation

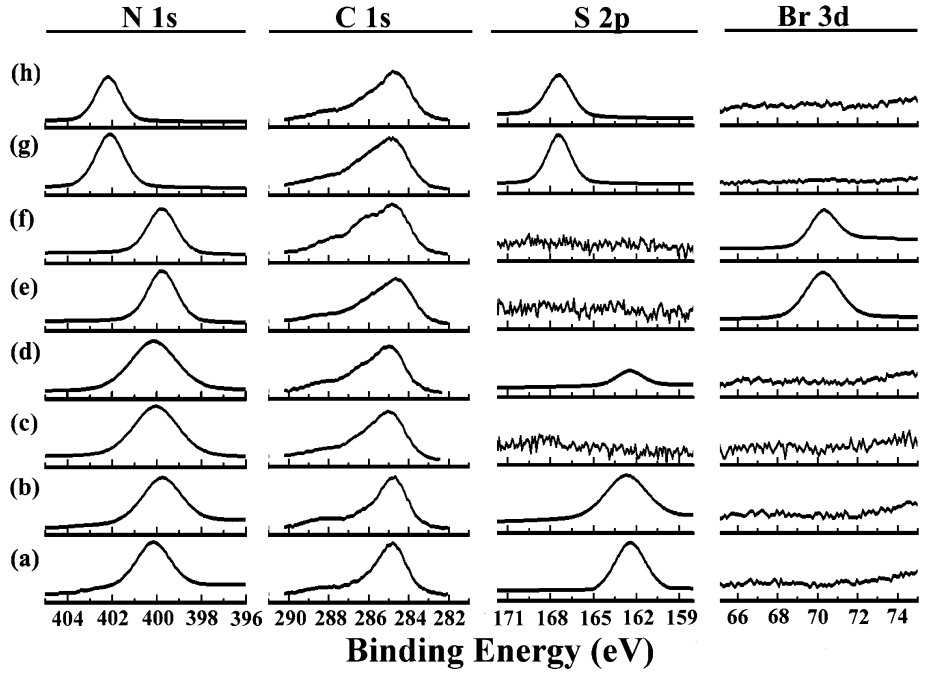

Figure 1. XPS spectra of various surface-modified stainless steel coupons in N 1s, C 1s, S 2p, and Br 3d regions: (a) pristine SUS, (b) UV-treated SUS, (c) SUS-D, (d) SUS-Si, (e) SUS-D-BiBB, (f) SUS-Si-BiBB, (g) SUS-D-pSBMA, and (h) SUS-Si-pSBMA.

range 450−490 nm. The respective adherent cell density from various fluorescent images was counted using ImagePro software.

Bacterial Adhesion Assay. Antibacterial activity assays were carried out using *Escherichia coli* and *Staphylococcus epidermidis*, the most common microbial pathogen encountered in orthopaedic infections.[10,39] *E. coli* and *S. epidermidis* were respectively cultured in a medium containing 3.0 mg/mL beef extract and 5.0 mg/mL bacto peptone. These cultures were incubated at 37 °C with constant agitation at 100 rpm until early stationary phase was reached, at a final *E. coli* concentration of 10^6 cells/mL for 12 h, and at a final S. *epidermidis* concentration of 1×10^9 cells/mL for 18 h.

Bare and functionalized SUS coupons were incubated with 75 wt % ethanol for 1 h at 25 °C and rinsed with PBS three times in a 24-well tissue culture plate. 1 mL of bacterial suspension was added to each well. The bacteria were then incubated with the samples for 6 h at 37 °C. Bacterial incubation was carried out for 6 h instead of 24 h because the post-implantation period of about 6 h has been identified as the period where prevention of bacterial adhesion is most critical to the long-term success of an implant.[40] The bacterial solution was then removed and each substrate was rinsed with deionized water for thrice to remove unattached bacteria. Bacteria attached to the substrate surfaces were stained with 200 μL of Live BacLight for 5 min. After rinsing with deionized water thrice, substrates with stained bacteria were detected with a CCD camera mounted on Olympus BX51 fluorescent microscope with a 20× objective lens. During observation, fluorescent illumination through a blue excitation fluorescence filter at the excitation range 450−490 nm was used. The numbers of adhered bacteria from various fluorescent images were counted using ImagePro software.

RESULTS AND DISCUSSION

Surface Modification of Stainless Steel. As shown in Scheme 1, the process for SUS surface modification could be divided into three stages. Prior to experiment, bare stainless steel surface was treated with ultraviolet light (UV) light to generate sufficient hydroxides on the surface. Bare stainless steel is first treated in each dopamine and organosilane solution to allow the formation of respective self-assembly layers on the substrate surface. Dopamine is identified as biomimetic adhesive pad proteins secreted by marine mussels that contains both functionalities catechol and amine functional groups, which are crucial for achieving adhesion to a wide spectrum of organic and inorganic materials. Research showed that it could easily immobilize on the substrate surface, forming surface-adherent polydopamine layers.[41,42] Dopamine is easily reacted under mildly basic conditions and a black brown basic solution was observed spontaneously in this study, which could be attributed to the formation of polydopamine layer containing quinone and other oxidized catechol groups.

Silanization method is another most commonly used immobilization method to form an adhesion layer for ATRP initiator attachment on inorganic metal surface. It has been reported in Fan et. al. (2005) for the use of organosilane as initiator in grafting poly(oligoethylene glycol) methacrylate from stainless steel via SI-ATRP.[41] Basically, it involved reactively deposited organosilane films with terminal functional groups that can be further modified with different linking moieties.[43] This silanization layer provided lateral structural stabilization through interchain cross-linking.[44] Warm air drying at 40 °C in this study promotes the condensation process of the silane on the post surface, thereby providing a more tightly packed configuration of the coupler molecules on the post surface,[45] according to Monticelli et. al. (2006). The end-chain amino groups were allowed for the subsequent attachment of alkyl bromide initiators.

The second stage was to graft the initiator, BIBB, onto the amino-terminated self-assembly surface, and eventually the SBMA monomers were polymerized from the BiBB-tethered surface *via* ATRP. This SI-ATRP approach takes advantage of strong interactions between catechol-based and organosilane-based anchoring agent with stainless steel metal. The linkage between the stainless steel surface and polySBMA is highly stable because of the covalent bondings between anchoring agents, BiBB initiators and SBMA monomers.

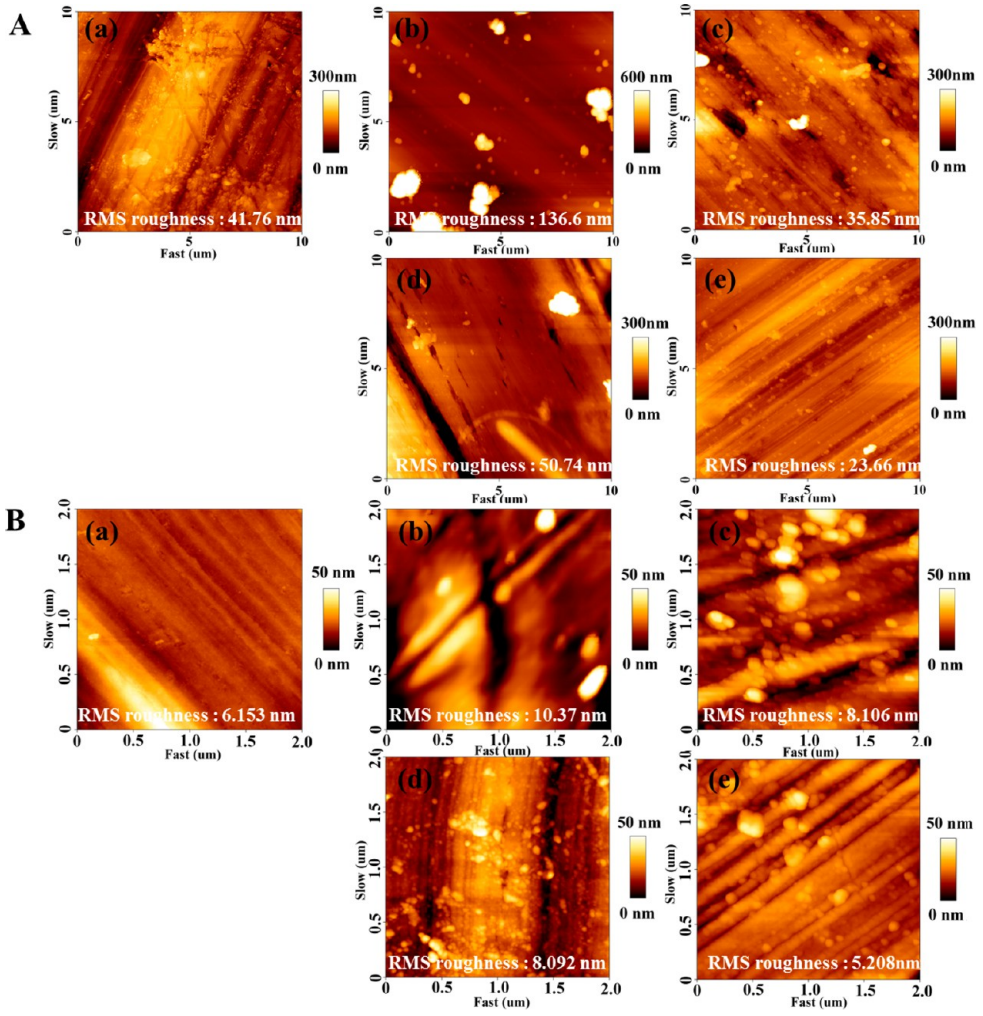

Figure 2. Tapping-mode AFM images of surface morphology and rms roughness of (a) pristine SUS, (b) SUS-D, (c) SUS-D-pSBMA, (d) SUS-Si, and (e) SUS-Si-pSBMA in dry state. The dimension of the scan images are (A) 10 μm × 10 μm and (B) 2 μm × 2 μm.

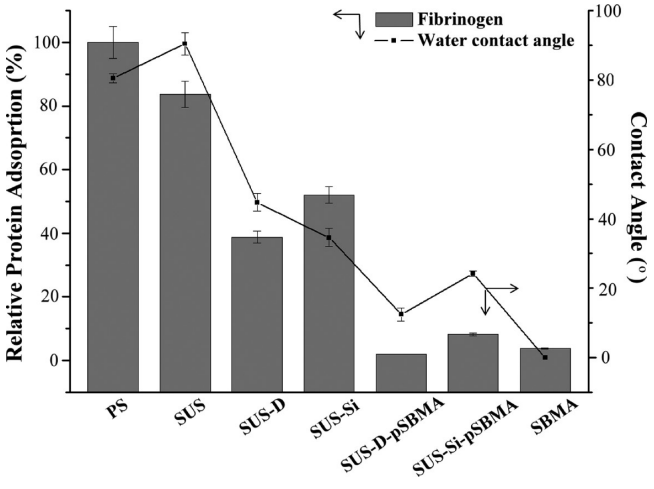

Figure 3. Changes in relative fibrinogen adsorption and water contact angle with various substrates, using tissue culture polystyrene (PS) as positive control and SBMA hydrogel as negative control.

Surface Characterization. The chemical structures and composition of SUS surfaces at various stages of surface modification was determined by XPS, as displayed in Figure 1. Stainless steel itself contains a variety of elements, with detectable N 1s peak at 400 eV, C 1s peak at 284.8 eV, and S 2p peak at 162 eV on the surface. After treated the stainless steel surface with 20 min UV radiation, the C−O content (C 1s peak signal at 286.1 eV) increased significantly from 16.9 to 25.8%, indicating the increased amount of hydroxides on the surface. Meanwhile successful anchoring of catechol dopamine and organosilane to SUS surface was indicated by the existence of a strong signal of N 1s peak at 400 eV. For example for dopamine-anchored SUS surface (SUS-D), a strong signal of N 1s peak with higher intensity at 400 eV was observed, which corresponded to the secondary amine groups present on SUS-D, showing that dopamine was anchored to the stainless steel surface. This anchoring agent formed a polydopamine interfacial layer with 15.6±2.2 nm in thickness on the SUS surface and therefore the native S 2p peak of stainless steel could not be detected. This thickness is in agreement with the range of polydopamine film thickness study as a function of immersion time, as conducted by Lee et. al. (2007).[42] On the other hand, for the silane-immobilized SUS surface (SUS-Si), a strong signal of N 1s peak at 400 eV was appeared and this indicates that silane was anchored to the SUS surface. The native S 2p peak signals (162 eV) attributed to stainless steel was still detectable on SUS-Si, but with very small intensity (Figure 1d). The persistence of the prominent S 2p signal in the spectrum suggests that the assembled silane film existed as a

dx.doi.org/10.1021/am4041256 | ACS Appl. Mater. Interfaces 2014, 6, 861−873

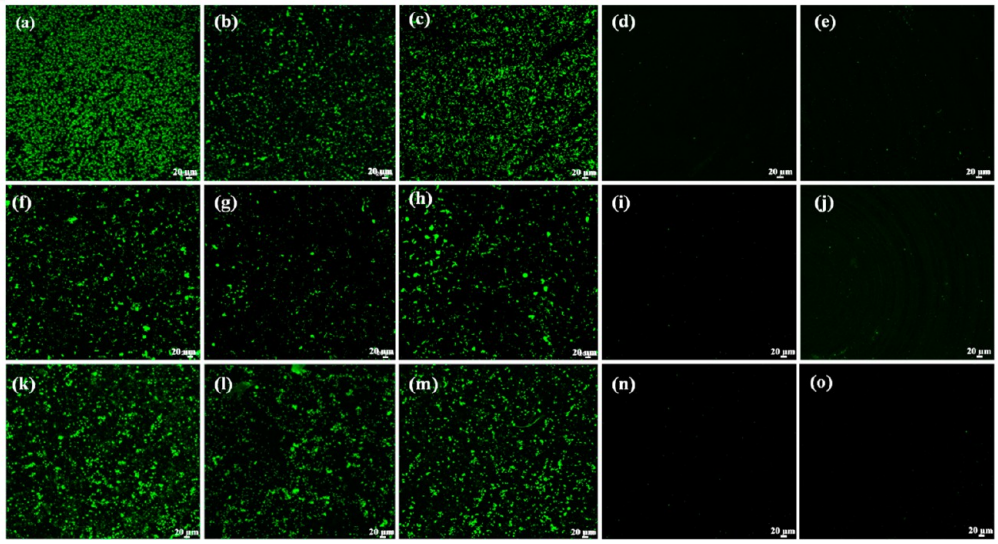

Figure 4. Fluorescent CLSM images of blood platelets adhered on (a) bare SUS, (b) SUS-D, (c) SUS-Si, (d) SUS-D-pSBMA, and (e) SUS-Si-pSBMA; blood erythrocytes adhered on (f) bare SUS, (g) SUS-D, (h) SUS-Si, (i) SUS-D-pSBMA, and (j) SUS-Si-pSBMA; and blood leukocytes adhered on (k) bare SUS, (l) SUS-D, (m) SUS-Si, (n) SUS-D-pSBMA, and (o) SUS-Si-pSBMA, respectively, under 200× magnification (scale bar = 20 μm).

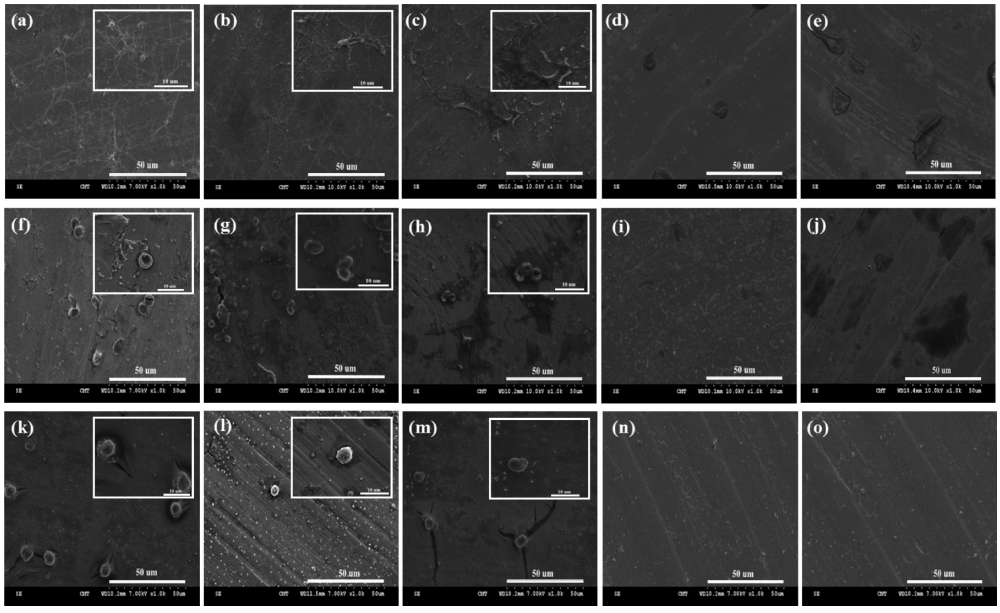

Figure 5. SEM images of blood platelets adhered and activated on (a) bare SUS, (b) SUS-D, (c) SUS-Si, (d) SUS-D-pSBMA, and (e) SUS-Si-pSBMA; blood erythrocytes adhered on (f) bare SUS, (g) SUS-D, (h) SUS-Si, (i) SUS-D-pSBMA, and (j) SUS-Si-pSBMA; and blood leukocytes adhered on (k) bare SUS, (l) SUS-D, (m) SUS-Si, (n) SUS-D-pSBMA, and (o) SUS-Si-pSBMA, respectively, under 1000× magnification (scale bar = 50 μm) and 3000× magnification (scale bar = 10 μm).

thin overlayer. This is in accordance with the ellipsometry measurement, whereby the thickness of silane monolayer showed only 1.0 ± 0.2 nm.

As shown in panels e and f in Figure 1, the appearance of the new signal assigned to Br 3d peak (70 eV) was observed, which indicated that 2-bromoisobutyryl bromide (BiBB) initiators could be covalently tethered to respective dopamine- (SUS-D) and silane-immobilized (SUS-Si) surfaces. When BiBB is tethered onto respective SUS-D and SUS-Si surfaces, the corresponding Br3d signals are discernible, in addition to reduced N1s signal. No S 2p peak was observed on both SUS-D-BiBB and SUS-Si-BiBB. After 24 h SI-ATRP of SBMA, the presence of the grafted polySBMA brushes on SUS-D-pSBMA and SUS-Si-pSBMA could be ascertained from the quartenary amine groups and the sulfonate groups, as evidenced by the binding energies of $-CH_2N(CH_3)_2CH_2-$ at 402 eV (N 1s) and $-CH_2SO_3$ at 167 eV (S 2p), respectively, as shown in panels g and h in Figure 1. The appearance of S 2p at 167 eV and shift of N 1s peak to higher binding energy (402 eV) indicated that polySBMA was successfully tethered to both SUS-D-BiBB and SUS-Si-BiBB. From the results of ellipsometry measurement, SUS-D-pSBMA and SUS-Si-pSBMA showed the grafted polymer film thickness of about 46.5 ± 1.8 nm and 24.8 ± 4.6 nm, respectively. By subtracting the thickness of the respective anchoring interfacial layer, the thickness of the polySBMA film could be in the range of 30.9 ± 0.4 nm (grown

dx.doi.org/10.1021/am4041256 | ACS Appl. Mater. Interfaces 2014, 6, 861−873

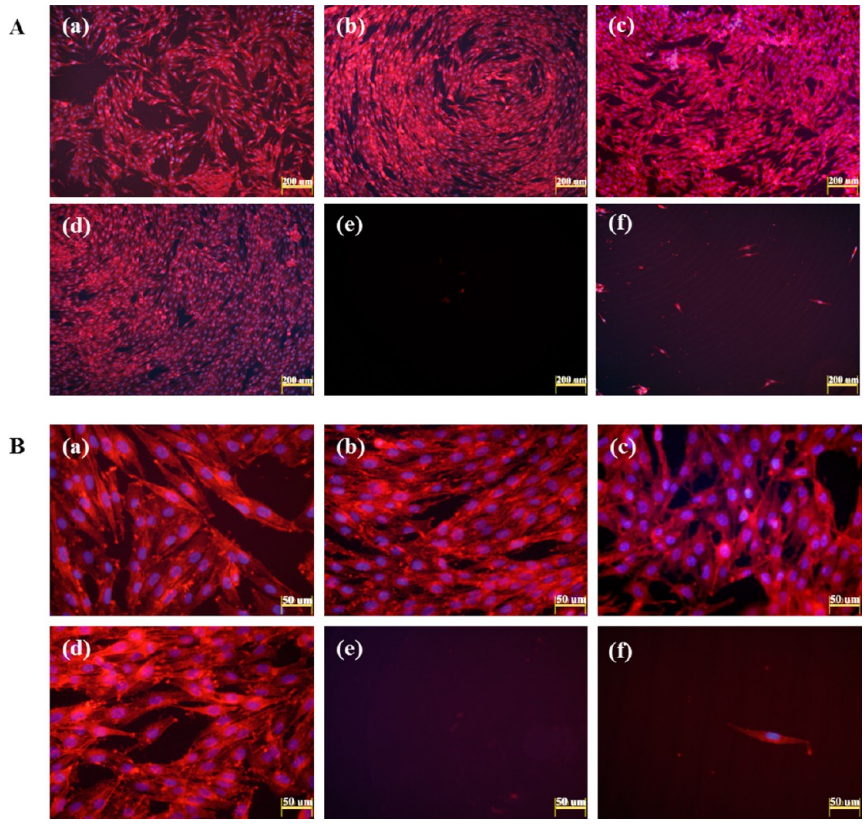

Figure 6. Fluorescent microscopic images of human MG63 osteoblast cells cultured on (a) control TCP, (b) bare SUS, (c) SUS-D, (d) SUS-Si, (e) SUS-D-pSBMA, and (f) SUS-Si-pSBMA, respectively, under (A) 100× magnification (scale bar = 200 μm) and (B) 400× magnification (scale bar = 50 μm).

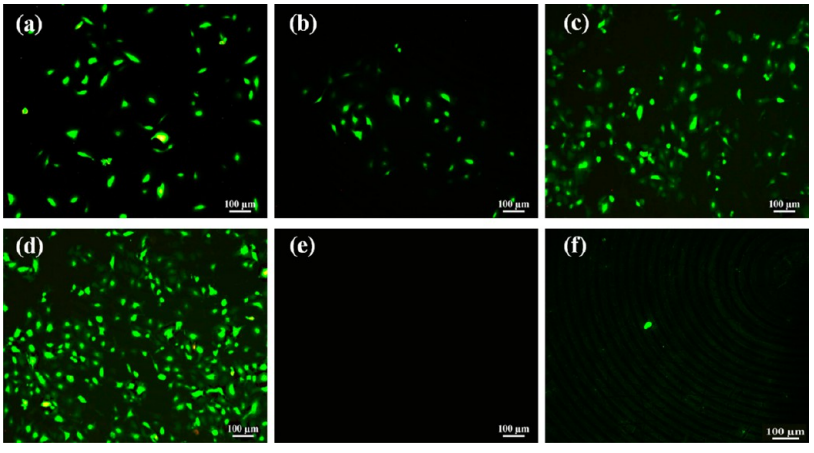

Figure 7. Fluorescent microscopic images of human HT1080 fibroblast cells cultured on (a) control TCP, (b) bare SUS, (c) SUS-D, (d) SUS-Si, (e) SUS-D-pSBMA, and (f) SUS-Si-pSBMA, respectively, under 100× magnification (scale bar = 100 μm).

from polydopamine layer) and 23.8 ± 4.4 nm (grown from silane monolayer). Because the thicknesses of the polySBMA layers are greater than the XPS penetration depth (about 10 nm), the Br3d signal is greatly reduced to undetectable level, giving rise to the disappearance of the Br3d peak signal. This high-resolution XPS spectral analysis demonstrated good agreement with the spectroscopic ellipsometry measurement for the structure of the grafted polymer ad-layers.

The surface morphology and roughness of pristine SUS, SUS-D, SUS-Si, SUS-D-pSBMA, and SUS-Si-pSBMA was observed by tapping-mode AFM (Figure 2). Figure 2a displays the topology of pristine SUS with rms roughness of ~41.76 nm (10 μm × 10 μm) and ~6.153 nm (2 μm × 2 μm) whereby patches, scratches and notches were detected on the substrate surface. The defect was probably due to the flaw production of SUS coupons from the machine as well as the deposition of organic contaminants on the surface since the pristine SUS was used without UV light treatment. Surface morphology and roughness of the dopamine and silane-functionalized surface before and after polySBMA polymerization were compared. From Figure 2b, an obvious increase in rms roughness of ~136.6 nm (10 μm × 10 μm) and ~10.37 nm (2 μm × 2 μm) with formation of multiple nanosized islands was observed in SUS-D. For SUS-Si, a relatively lower rms roughness value of

dx.doi.org/10.1021/am4041256 | ACS Appl. Mater. Interfaces 2014, 6, 861−873

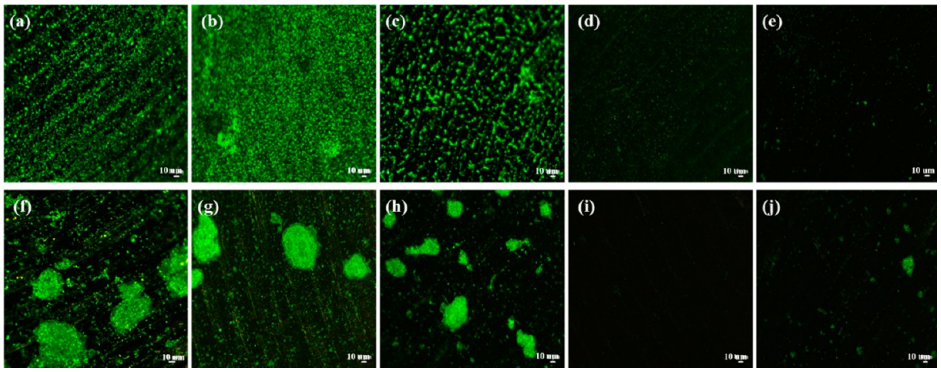

Figure 8. Fluorescent microscopic images of *E. coli* attachment on (a) bare SUS, (b) SUS-D, (c) SUS-Si, (d) SUS-D-pSBMA, and (e) SUS-Si-pSBMA; and *S. epidermidis* attachment on (f) bare SUS, (g) SUS-D, (h) SUS-Si, (i) SUS-D-pSBMA, and (j) SUS-Si-pSBMA, respectively, under 200× magnification (scale bar = 10 μm).

~50.74 nm (10 μm × 10 μm) and ~8.092 nm (2 μm × 2 μm) was detected (Figure 2d). These observations propose that a condensed polydopamine layer formed on the dopamine-immobilized surface with nanoscale phase aggregation, whereas a smoother and uniform layer of organosilane was generated on the silane-immobilized surface. After surface polymerization of SBMA, the rms roughness values for both SUS-D-pSBMA (Figure 2c) and SUS-Si-pSBMA (Figure 2e) reduced to 35.85 nm (10 μm × 10 μm) and 8.106 nm (2 μm × 2 μm); 23.66 nm (10 μm × 10 μm) and 5.208 nm (2 μm × 2 μm), respectively. As shown in the figure, compared to SUS-D-pSBMA which exhibited a formation of non-homogeneous polySBMA layers with randomly distributed domains, a tightly packed and orderly distribution of polymer brushes was detected along the surface of SUS-Si-pSBMA. A significant variation in topology and roughness depicted in pristine SUS and each functionalized SUS could be correlated with surface coverage and the conformational structure of coupled dopamine and silane interfacial layers as well as the grafted polySBMA layer.

Static water contact angle data of these surfaces are summarized in Figure 3. The changes in the surface water contact angle also confirmed the sequential formation of the initiator and polymer layers. Prior to initiator coupling and SI-ATRP, freshly cleaned bare SUS substrates were hydrophobic with static water contact angle of about 90.5±3.2° (Figure 3), which decreased to an average value of 44.7 ± 2.5 and 34.6 ± 2.6° after immobilization of respective anchoring agents of catechol dopamine and organosilane. When BiBB initiator immobilized on both SUS-D and SUS-Si surfaces, the surface water contact angles increased to 80.2 ± 1.1° and 72.7 ± 0.8°, respectively. After 24 h SI-ATRP of SBMA, the contact angles for both SUS-D-pSBMA and SUS-Si-pSBMA surfaces decreased to 12.5 ± 1.9° and 24.2 ± 0.8°, indicating an increase in hydrophilicity due to the grafted polySBMA brushes. Therefore, it is concluded that grafting of stainless steel surface with polySBMA made the SUS surfaces more hydrophilic as shown by the drastic drop in water contact angle.

Nonspecific Plasma Protein Adsorption. In general, it is acknowledged that nonspecific protein adsorption is the first event in blood-biomaterial interactions, which may give rise to the provocation of the intrinsic cascade, leading to immune response, thrombosis and embolism at the blood contact side of implant devices.[46,47] Thus a good nonspecific protein-fouling resistance is one of the key requirements for preparing non-bioadhesive biomaterials. Fibrinogen (Fg) plays vital part in mediating surface-stimulated platelets adsorption and activation among plasma proteins in human blood plasma. Fg in blood plasma is often used as a model protein to assess the ability of a non-bioadhesive surface to resist its adsorption, because it is markedly essential for platelet aggregation as it can attach to the platelet GP IIb/IIIa receptor.[8] Therefore, in this study, the protein-fouling resistant property of functionalized SUS surfaces was tested by measuring the level of Fg adsorption using ELISA and the data were shown in Figure 3.

The ability of the functionalized substrates to reduce the amount of fibrinogen adhesion was compared with a reference polymer polystyrene (100% of relative Fg adsorption). Control data for bare stainless steel under the same experimental condition is also reported (Figure 3). As compared with SUS (about 85% of relative Fg adsorption), the relative protein adsorption on both SUS-D and SUS-Si were dropped to approximately 40 and 50%, respectively. Because stainless steel itself has a very high surface energy, the strong affinity of its surface for protein is well known[2] in which the metal surface binds soluble proteins irreversibly through mixed charge interactions. An obvious reduction of Fg adsorption level was observed on the polySBMA-grafted SUS, with SUS-D-pSBMA (1%) accounted for the lowest Fg adsorption, compared to SUS-Si-pSBMA (8%). The results show that polySBMA-grafted surfaces prepared from the silanization method could only reduce protein adsorption to some degree, whereas polySBMA-grafted from SUS-D surface could effectively reduce protein adsorption to almost non-fouling level. The electrical neutrality and absence of hydrogen-bond donors in the grafted zwitterionic polySBMA play a determining factor in minimizing both the electrostatic interactions and hydrogen bonding interactions with plasma proteins.[31,37] The formation of the bounded water layer on highly hydrated surface[33,34] was also demonstrated as a crucial issue to repel plasma proteins on polySBMA-grafted surfaces.

Human Blood-Platelet and Blood-Cell Adhesion. Plasma proteins, blood platelets, and blood cells are the primary components of blood and function as signaling and self-sustaining processes in human body. There is an interlinked mechanism of plasma protein, blood platelet and blood cell attachment.[8] Typically, a multi-step action of plasma protein, blood platelet and blood cell adhesion distinctly influence the short-term and long-term host responses stimulated by the blood-contacting SUS implants. Thrombus formation is one of the most serious host responses to implanted biomaterials. Because stainless steel do not have sufficient blood compatibility and anti-thrombogenicity, it is important to design an

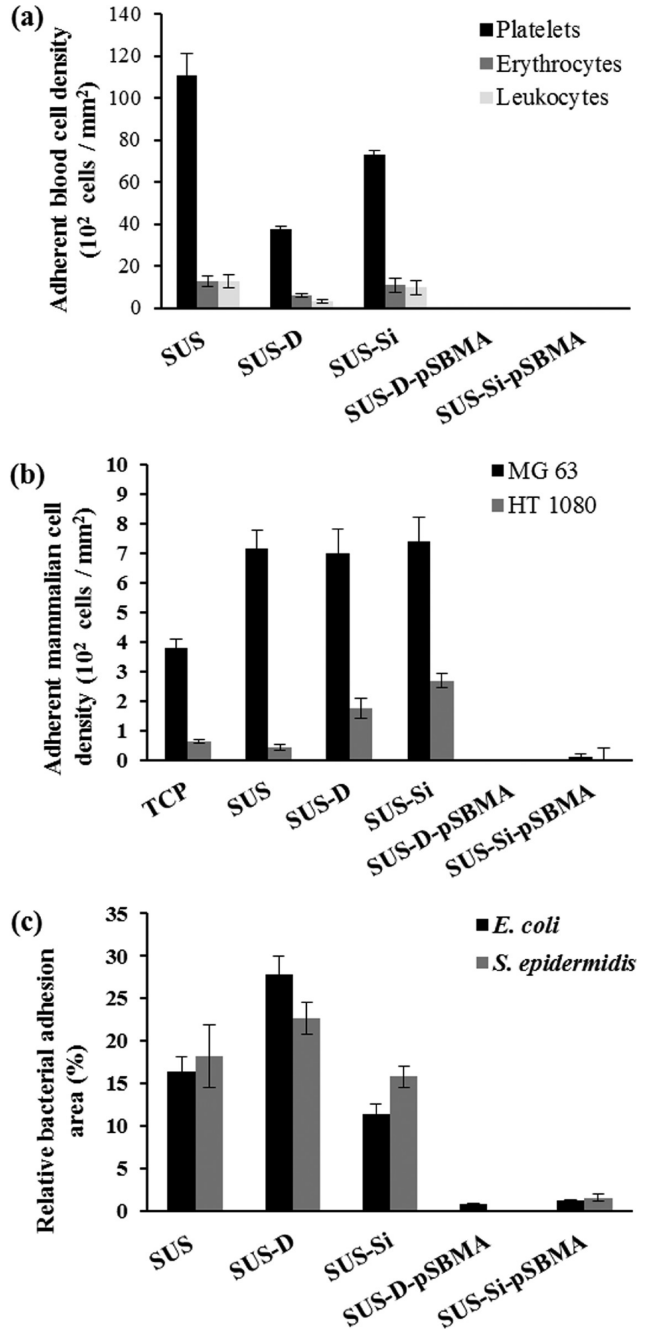

Figure 9. Statistical analysis of (a) adherent blood platelets and blood cells density, (b) adherent human MG63 osteoblast and HT1080 fibroblast cells density, and (c) percentage of occupied area of *E. coli* and *S. epidermidis* attachment on various surface-modified stainless steel coupons.

anti-bioadhesive surface for the metal surface to avoid thrombus formation. Inflammatory-thrombotic intricacies correlated with biomaterials are linked discernibly to their capability to trigger platelets activation. There is an agreement that the rapidly adsorbed proteins, especially fibrinogen, play a critical role in platelet adhesion. In general, the ability of a surface to resist fibrinogen adsorption, is a prerequisite for that surface to resist blood platelet adhesion and activation.[46,47]

Figure 4 shows confocal laser scanning microscopy (CLSM) images of blood platelets and blood cells that adhered to the prepared substrate surfaces. Many adherent blood platelets and blood cells were observed on SUS, SUS-D and SUS-Si. CLSM images revealed that almost no or little blood platelets, erythrocytes and leukocytes adhesion was detected on the surfaces of SUS-D-pSBMA and SUS-Si-pSBMA (Figure 4d, e, i, j, n, and o). Apparently the outstanding bio-inert nature of zwitterionic sulfobetaine structure can be accomplished by grafting the surface with polySBMA brushes to completely resist blood platelets and blood cells adhesion.

The morphology of adhering and activated platelets on the substrates in contact with recalcified PRP solution was observed from the SEM images at 1000x and 3000x magnification (Figure 5). It is clearly observed in Figure 5a–c that many platelets adhered, aggregated, and were activated as shown by the well-spread pseudopods on SUS, SUS-D and SUS-Si, indicating the formation of thrombosis on the substrate surfaces. According to Gorbet and Sefton (2004), a structural variation in platelet takes place upon activation, with the formation of platelet microparticles via exocytotic budding, which leads to the exposure of high-affinity attachment site for soluble fibrinogen. Tethering of fibrinogen to GPIIb/IIIa results in platelet activation and agglomeration;[8] meanwhile mediating leukocyte attachment through interaction with GPIIb/IIIa and cD11b,[48] giving rise to the formation of platelet–leukocyte aggregates.[8]

As shown in images d and e in Figure 5, no platelets adhered and activated on both SUS-D-pSBMA and SUS-Si-pSBMA surfaces. The excellent performance of zwitterionic polySBMA-grafted surfaces with remarkably suppressed platelet adherence and activation could be attributed to its capability to significantly suppress fibrinogen adhesion from blood plasma. The reduction of relative fibrinogen adsorption levels below 10% on polySBMA-grafted surfaces is comparable to the level below 10 ng/cm^2. According to Horbett et al., diminishing the levels of plasma protein adsorption to below 10 ng/cm^2 can efficaciously restrain the platelets adhesion and activation from the bloodstream.[46,47]

It should be noted that biomaterials community most often focuses on the study of platelet interactions in platelet-rich plasma but seldom delve into the interactions between leukocytes and platelets. In fact, the molecular links between inflammation and thrombosis are undeniable. Inflammation, as delineated by a leukocyte response may contribute to the capability of released inflammatory mediators to activate platelets; and by stimulating the aggregate formation between leukocytes and platelets.[8,49] Thus reducing attachment of leukocytes also plays a determining factor in inhibiting the foreign body response to the implanted biomaterial. The extent of human blood cell attachment was scrutinized by direct contact of human blood erythrocytes and leukocytes with each functionalized metal surface. The SEM results show a full-scale attached and aggregated erythrocytes and leukocytes at the blood contact site on SUS, SUS-D and SUS-Si (Figure 5f, g, h, k, l, and m). On the other hand, almost clean substrate surfaces with no erythrocytes and leukocytes attachment were observed on both SUS-D-pSBMA and SUS-Si-pSBMA surfaces (Figure 5i, j, n, and o). The results confirmed the previous hypothesis that the charge-balanced surface from zwitterionic groups of polySBMA can provide excellent bioadhesive resistance as the electrostatic attractive forces and hydrophobic interactions between the biomaterials and blood cells have been suppressed.[31]

Statistical analysis of relative blood platelet adhesion and blood cell attachment are presented in Figure 9a. The numbers

dx.doi.org/10.1021/am4041256 | ACS Appl. Mater. Interfaces 2014, 6, 861–873

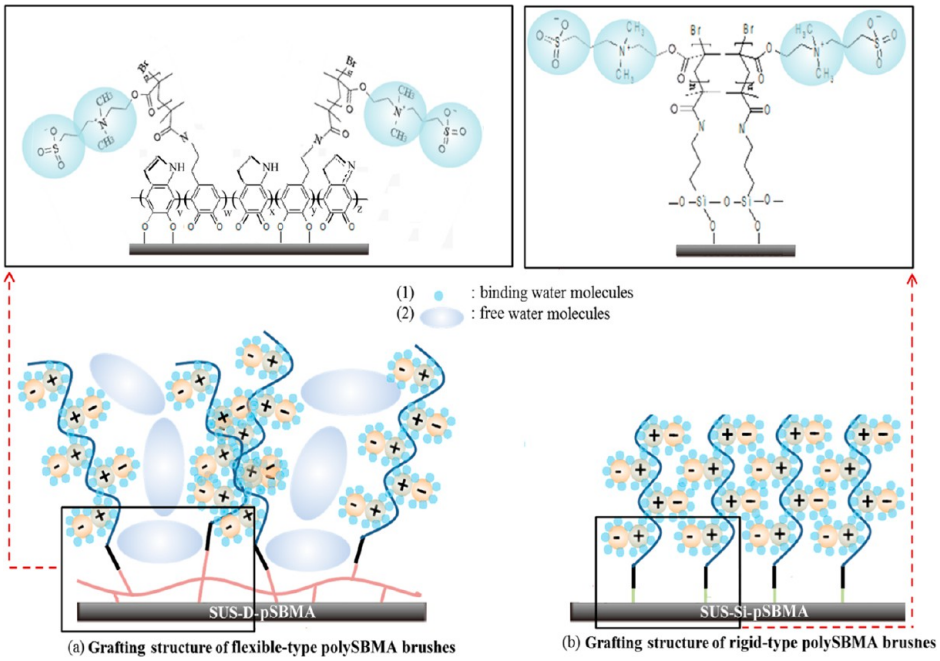

Figure 10. Plausible illustration of the hydrated chain conformation of prepared polySBMA brushes from (a) dopamine- and (b) silane-assembly layers. The polydopamine layer contained possible repeating unit of quinone and oxidized catechol groups, which were randomly distributed along the interfacial layer.

of adhered platelets, erythrocytes, and leukocytes on the bare SUS surface were about 11.1×10^3, 1.3×10^3, and 1.2×10^3 (cells per mm^2), respectively. A significant decrease in the number of adhering platelets and blood cells was observed on the polySBMA-grafted SUS, with only 32 and 46 (cells per mm^2) adhering platelets, 10 and 15 (cells per mm^2) adhering erythrocytes, and 9 and 12 (cells per mm^2) leukocytes on respective SUS-D-pSBMA and SUS-S-pSBMA surfaces.

Evaluation of Osteoblast and Fibroblast Cell Attachment. Up to human tissues level, prevention of mammalian cells adhesion and spreading is another important parameter for implant engineering. In order to avoid the subsequent second damage to the adjacent cells and tissues due to removing implant from the just healed soft tissues, it is important to make the implant surface to be cell adhesion resistance. The human cell and tissue response to polySBMA grafted SUS surfaces was assessed by studying the resistance of polySBMA to surrounding mammalian cell attachment using MG63 osteoblast- and HT1080 fibroblast-like cells as model cell; the two common cell populations that are in vivo in contact with biomaterials.

Figure 6 shows the comparative results of human MG63 osteoblast cell adhesion assay cultured in the presence of bare and functionalized SUS substrates. As shown in the figure, the bare SUS surface favored MG63 osteoblasts adhesion with a good cell spreading. Bare SUS has high surface energy that favors high protein adhesion, thus exhibiting good mammalian cell attachment and growth. It should be noted that the interactions between cells and biomaterials are usually directed by the absorbed plasma proteins on the interface, whereby the adsorbed proteins dictate and initiate cell response. When a cell contacts a protein-immobilized surface, it interacts with this adsorbed protein layer and not the base material itself.[50] The MG63 cells grow along with the ripples of stainless steel (Figure 6b). Therefore, the cell morphology appeared to be slightly different with ordinary MG63 cells growing on tissue culture plate (TCP) (Figure 6a). Cells were able to adhere and proliferate on SUS, SUS-D and SUS-Si surfaces and the cell coverage on the functionalized surfaces were more uniform and extensive than that observed for TCP. On the other hand, MG63 cell growth and attachment were remarkably suppressed on both SUS-D-pSBMA and SUS-Si-pSBMA (Figure 6e, f), indicating that zwitterionic polySBMA does not support cell attachment.

The fluorescent images of attached human HT1080 fibroblast cells on bare and functionalized SUS are displayed in Figure 7 at 100× magnification. HT1080 cells adhered and spread over TCP, SUS, SUS-D and SUS-Si surfaces into a confluent-like shape. However, almost no cell was found on SUS-D-pSBMA and little cells were adhered to the SUS-Si-pSBMA surfaces. Cellular behavior and response on biomaterial surfaces depends upon implant−cell interactions, correlated with surface properties such as surface hydrophilicity and charge neutrality. The SUS-D and SUS-Si with cationic amino groups on the surface were shown to promote cell adhesion and proliferation. It could be observed from both Figures 6 and 7 that SUS-D and SUS-Si showed larger cell coverage in comparison to bare SUS. Both MG63 and HT1080 cell growth on the SUS-D-pSBMA and SUS-Si-pSBMA surfaces was restrained in comparison to that on SUS, SUS-D, and SUS-Si surfaces, which was in agreement with the assumption that zwitterionic surfaces with a total charge neutrality constituted from ion pairings between ammonium cation and sulfoanion that could perform the antibioadhesive properties. Nevertheless, although polySBMA-grafted surface does not support cell adhesion, it does not adversely affect the viability of cells.[36]

The trends in the adherent cell coverage on various substrate surfaces are in accordance with the quantitative cell count results. Statistical analysis of relative cell adhesion on substrate surface is revealed in Figure 9b. MG63 cells readily attached on bare SUS at average density of approximately 720 cells/mm^2, whereas SUS-D and SUS-Si surfaces supported robust MG63

dx.doi.org/10.1021/am4041256 | ACS Appl. Mater. Interfaces 2014, 6, 861−873

cell attachment of around 700 and 750 cells/mm^2, respectively. Both SUS-D-pSBMA and SUS-Si-pSBMA surfaces supported poor cell attachment, with only 2 cells and 13 cells adhered on each mm^2 surface area. On the other hand, poor HT1080 cell attachment was observed on bare SUS surface, with the adherent cell density accounted for 44 cells/mm^2, compared to 177 and 270 cells/mm^2 on both SUS-D and SUS-Si surfaces. About 99% reduction in cell adhesion density was observed on both SUS-D-pSBMA and SUS-Si-pSBMA, whereby only 3 cells per mm^2 attached on SUS-Si-pSBMA surface and no HT1080 cell was attached on SUS-D-pSBMA.

Antibacterial Efficacy. As stated previously, a significant complication in implant surgery that leads to implant failure is bacterial infection. Once bacteria cells adhere to the surface of the implant, a biofilm generally formed to resist host defense mechanisms and administered antibiotics.[15] Antibacterial surfaces that prevent the growth of biofilms are an alternative way to inhibit the spread of biomaterial infections. To achieve this, the materials are required to avoid the primary adhesion of living planktonic bacterial cells from the surroundings by repelling the microbes from attaching to the surface. To evaluate the antibacterial activity of polySBMA-grafted SUS surfaces, two bacterial species, *Escherichia coli* and *Staphylococcus epidermidis*, which are commonly associated with infections of orthopedic implants devices[10] were used in this study.

The qualitative images of accumulated *E. coli* and *S. epidermidis* on substrate surfaces are displayed in Figure 8 at 200× magnification. The bare SUS showed the robust bacterial growth on the substrate surface after 6 h incubation in the bacterial culture media. Initial stage of non-specific protein adhesion could favor the bacterial adhesion onto hydrophobic biomaterial surface, due to the presence of protein content on the outer bacterial cell membrane. Nevertheless, *E. coli* and *S. epidermidis* display different morphology upon adhesion, whereby *E. coli* tend to spread and scatter over the surface while *S. epidermidis* tend to cluster together with a full-scale attachment. Bacteria cells grown on SUS-D and SUS-Si are well-proliferated, indicating that these surfaces exhibit low antibacterial activity. On the other hand, the degree of bacterial attachment on SUS-D-pSBMA and SUS-Si-pSBMA decreased drastically, with SUS-D-pSBMA appears to have higher efficacy in preventing the bacterial adhesion. It should be noted that both *E. coli* and *S. epidermidis* with charged surfaces have low attachment tendency to the electrically neutral zwitterionic polySBMA. Besides that, significant inhibition of bacteria growth by polySBMA grafting could be attributed to the hydration layers which could minimize the bacteria adhesion.

Statistical analysis of relative bacterial coverage on various substrate surfaces is revealed in Figure 9c. All tested polySBMA-grafted surfaces showed marked reduction above 98% in the bacterial percentage coverage in relative to that for bare SUS. SUS-D-pSBMA surface can resist the bacterial adhesion to greater extent whereby only 0.8% *E. coli* adhesion and 0.02% *S. epidermidis* adhesion were observed on these substrate surfaces. Nevertheless SUS-Si-pSBMA surface could still be adhered by significant amount of bacteria (1.2% *E. coli* adhesion and 1.5% *S. epidermidis* adhesion, respectively).

Correlation of Grafting Coverage and Conformational Structure of PolySBMA Brushes with Hydration Capability. It is hypothesized that the excellent performance in the anti-bioadhesion of zwitterionic polymers are tightly correlated with the hydration layer near the interface, as the tightly bound water layer forms a physical and energetic barrier to prevent proteins, cells and microbial adhesion on the surface. Figure 10 depicts a hypothetical illustration of the hydrated chain conformation of prepared polySBMA brushes, respectively, from dopamine-based and organosilane-based assembly layers. As shown in panels a and b in Figure 10, water molecules are polarized around the zwitterionic sulfobetaine groups, whereby these positive and negative charged units bind water molecules strongly and stably via electrostatically induced hydration.

On the basis of the results above, polySBMA brushes grafted from immobilized polydopamine interfacial layers achieved an overall better bioadhesion resistance. An overall thicker polySBMA brushes were grown from polydopomine-anchored surface, which leads to a larger surface grafting coverage than that of polymer brushes grafted from silane-anchored SUS. This assumption was in agreement with the surface morphology of SUS-D-pSBMA and SUS-Si-pSBMA as revealed in AFM analysis (Figure 2c, e). Thus it could be one of the reasons for the higher biofouling resistance efficiency conferred by SUS-D-pSBMA. In fact, even though under similar experimental condition, by using silane as anchoring agent, the efficacy of grafting polySBMA brushes successfully from stainless steel is lower, showing that polySBMA brushes prepared via silane-surfaced immobilization method is not an effective approach to prepare a zwitterionic-based stainless steel.

Besides that, as illustrated in Figure 10a, more free water molecules could be retained around the surface of flexible-type polySBMA brushes growing from the polydopamine interfacial layers. PolySBMA brushes grown from dopamine-immobilized surface are possibly loosely packed in molecular-level, and this occurrence could lead to a larger space for free water molecules flowing between polymer brushes, producing a thick hydration layer at the surface. The enhanced interfacial hydration capacity and larger repulsive hydration forces could therefore result in an increase in their resistance efficiency to non-specific bioadhesion. In contrast, rigid-type polySBMA brushes could be generated from uniform silanized layer with a thin hydration layer as the polymer brushes are not free about to move around (Figure 10b). It should be noted that the packing or orientation of the attached polymer brushes plays a determining factor in influencing the coverage of retained free water molecules. Therefore, the flexible brush conformation of SUS-D-pSBMA surface is deduced to be more effective in preventing bioadhesion. Nevertheless, hydration in polymer brushes is far more complex than the depicted figure and further studies need to be carried out to investigate the detailed conformational structure of the polymer brushes, including the durability of the anti-bioadhesive properties conferred by the grafted pSBMA for long-term implantation.

CONCLUSIONS

Both XPS and water contact angle data ascertained successful initiator immobilization and polySBMA grafting from stainless steel surface via SI-ATRP. AFM results suggest that the different conformational structures of grafted polySBMA layers would form from different preparation approach. The grafted zwitterionic polySBMA brushes showed good anti-fibrinogen adsorption, anti-blood cells adhesion and platelets activation, good resistance to human MG63 osteoblast and HT1080 fibroblast cells attachment, as well as good anti-bacterial adhesion. The ability of polySBMA graftings to resist fibrinogen, blood platelets and leukocytes adsorption makes polySBMA-grafted stainless steel a very promising thrombo-

resistant biomaterial. Besides that, active infections caused by *Escherichia coli* and *Staphylococcus* could be subsided because of the improved antibacterial property from polySBMA brushes. Therefore, polySBMA-grafting is promising and can be applied to stainless steel implants as they would not irritate the surrounding tissues and incite excessive inflammatory response in human body.

Two initiator immobilization approaches: catechol dopamine- and organosilane-based immobilization, were also compared to graft ATRP initiators onto stainless steel surfaces for polySBMA polymerization. Results show that polySBMA grafted from polydopamine interfacial layers achieved better bioadhesion resistance than from silane-based assembly layer. This could be attributed to the conformational structure of the anchoring agent assembly layer, which plays a determining factor in the formation of flexible, well-spaced polySBMA brushes with greater hydration capacity and grafting coverage. Nevertheless, more experiments on the long-term stability of polySBMA grafting need to be conducted for future study before actual in vivo implementation of polySBMA-grafted stainless steel.

■ ASSOCIATED CONTENT

Supporting Information

Spectroscopic ellipsometry measurements of SUS-D, SUS-D-pSBMA, SUS-Si, and SUS-Si-pSBMA substrates. This material is available free of charge via the Internet at http://pubs.acs.org/

■ AUTHOR INFORMATION

Corresponding Authors

*E-mail: ychang@cycu.edu.tw.
*E-mail: cesunym@saturn.yzu.edu.tw

Author Contributions

These authors contributed equally to this work.

Notes

The authors declare no competing financial interest.

■ ACKNOWLEDGMENTS

The authors express their sincere gratitude to the Center-of-Excellence (COE) Program on Membrane Technology from the Ministry of Education (MOE), R.O.C., the project of Outstanding Professor Research Program in the Chung Yuan Christian University (CYCU-00RD-RA002-11757), and the National Science Council (NSC 100-2628-E-033-001-MY3) for their financial support.

■ REFERENCES

(1) Lane, W. A. *Brit. Med. J.* **1895**, *1*, 861−863.
(2) Helsen, J. A.; Breme, H. J. *Metals as Biomaterials*; New York: Wiley, 1998; pp 265−290.
(3) Shahryari, A.; Omanovic, S.; Szpunar, J. A. *Mater. Sci. Eng., C* **2008**, *28*, 94−106.
(4) Lacefield, W. R. *Ann. NY. Acad. Sci.* **1988**, *523*, 72−80.
(5) Horbett, T. A. *Cardiovasc. Pathol.* **1993**, *2*, 1375−1485.
(6) Andrade, J. D.; Nagaoka, S.; Cooper, S.; Okano, T.; Kim, S. W. *Am. Soc. Artif. Intern. Org. J.* **1987**, *10*, 75−84.
(7) Courtney, J. M.; Lamba, N. M. K.; Sundaram, S.; Forbes, C. D. *Biomaterials* **1994**, *15*, 734−744.
(8) Gorbet, M. B.; Sefton, M. V. *Biomaterials* **2004**, *25*, 5681−5703.
(9) Gristina, A. G. *Science* **1987**, *237*, 1588−1595.
(10) Campoccia, D.; Montanaro, L.; Arciola, C. R. *Biomaterials* **2006**, *27*, 2331−2339.
(11) von Eiff, C.; Jansen, B.; Kohnen, W.; Becker, K. *Drugs* **2005**, *65*, 179−214.
(12) Costerton, J. W.; Stewart, P. S.; Greenberg, E. P. *Science* **1999**, *284*, 1318−1322.
(13) An, Y. H.; Friedman, R. J. *J. Biomed. Mater. Res.* **1998**, *43*, 338−348.
(14) Baltimore, R. S.; Mitchell, M. J. *Infect. Dis.* **1980**, *141*, 238−247.
(15) Jensen, E. T.; Kharazmi, A.; Lam, K. *Infect. Immun.* **1990**, *58*, 2383−2385.
(16) Khoury, A. E.; Lam, K.; Ellis, B.; Costerton, J. W. *ASAIO J.* **1992**, *38*, M174−178.
(17) Hetrick, E. M.; Schoenfisch, M. H. *Chem. Soc. Rev.* **2006**, *35*, 780−789.
(18) Castner, D. G.; Ratner, B. D. *Surf. Sci* **2002**, *500*, 28−60.
(19) Brash, J. L. *J. Biomater. Sci.: Polym. Ed.* **2000**, *11*, 1135−1146.
(20) Zhang, F.; Kang, E. T.; Neoh, K. G.; Wang, P.; Tan, K. L. *Biomaterials* **2001**, *22*, 1541−1548.
(21) Husseman, M.; Malmstrom, E. E.; McNamara, M.; Mate, M.; Mecerreyes, D.; Benoit, D. G.; Hedrick, J. L.; Mansky, P.; Huang, E.; Russell, T. P.; Hawker, C. J. *Macromolecules* **1999**, *32*, 1424−1431.
(22) Pyun, J.; Kowalewski, T.; Matyjaszewski, K. *Macromol. Rapid. Commun.* **2003**, *24*, 1043−1059.
(23) Matyjaszewski, K. *Macromolecules* **2012**, *45*, 4015−4039.
(24) Feng, W.; Brash, J. L.; Zhu, S. P. *Biomaterials* **2006**, *27*, 847−855.
(25) Iwasaki, Y.; Ishihara, K. *Anal. Bioanal. Chem.* **2005**, *381*, 534−546.
(26) Li, G.; Cheng, G.; Xue, H.; Chen, S.; Zhang, F.; Jiang, S. *Biomaterials* **2008**, *29*, 4592−4597.
(27) Chiang, Y. C.; Chang, Y.; Higuchi, A.; Chen, W. Y.; Ruaan, R. C. *J. Membr. Sci.* **2009**, *339*, 151−159.
(28) Chang, Y.; Shih, Y. J.; Lai, C. J.; Kung, H. H.; Jiang, S. Y. *Adv. Funct. Mater.* **2013**, *23*, 1100−1110.
(29) Lowe, A. B.; McCormick, C. L. *Chem. Rev.* **2002**, *102*, 4177−4189.
(30) Chang, Y.; Chen, S. F.; Zhang, Z.; Jiang, S. Y. *Langmuir* **2006**, *22*, 2222−2226.
(31) Chang, Y.; Shu, S. H.; Shih, Y. J.; Chu, C. W.; Ruaan, R. C.; Chen, W. Y. *Langmuir* **2010**, *26*, 3522−3530.
(32) Chang, Y.; Chang, Y.; Higuchi, A.; Shih, Y. J.; Li, P. T.; Chen, W. Y.; Tsai, E. M.; Hsiue, G. H. *Langmuir* **2012**, *28*, 4309−4317.
(33) Zhang, Z.; Chao, T.; Chen, S. F.; Jiang, S. Y. *Langmuir* **2006**, *22*, 10072−10077.
(34) Chang, Y.; Liao, S. C.; Higuchi, A.; Ruaan, R. C.; Chu, C. W.; Chen, W. Y. *Langmuir* **2008**, *24*, 5453−5458.
(35) Chen, S. F.; Li, L. Y.; Zhao, C.; Zheng, J. *Polymer* **2010**, *51*, 5283−5293.
(36) Zhang, Z.; Chao, T.; Liu, L.; Cheng, G.; Ratner, B. D.; Jiang, S. *J. Biomater. Sci. Polym. Ed.* **2009**, *20*, 1845−1859.
(37) Chang, Y.; Chang, W. J.; Shih, Y. J.; Wei, T. C.; Hsiue, G. H. *ACS Appl. Mater. Interfaces* **2011**, *3*, 1228−1237.
(38) Chen, S. H.; Chang, Y.; Lee, K. R.; Wei, T. C.; Higuchi, A.; Ho, F. M.; Tsou, C. C.; Ho, H. T.; Lai, J. Y. *Langmuir* **2012**, *28*, 17733−17742.
(39) Tsuchiya, H.; Shirai, T.; Nishida, H.; Murakami, H.; Kabata, T.; Yamamoto, N.; Watanabe, K.; Nakase, J. *J. Orthop. Sci.* **2012**, *17*, 595−604.
(40) Poelstra, K. A.; Barekzi, N. A.; Rediske, A. M.; Felts, A. G.; Slunt, J. B.; Grainger, D. W. *J. Biomed. Mater. Res.* **2002**, *60*, 206−215.
(41) Fan, X.; Li, L.; Dalsin, J. L.; Messersmith, P. B. *J. Am. Chem. Soc.* **2005**, *127*, 15843−15847.
(42) Lee, H.; Dellatore, S. M.; Miller, W. M.; Messersmith, P. B. *Science* **2007**, *318*, 426−430.
(43) Matinlinna, J. P.; Areva, S.; Lassila, L. V. J.; Vallittu, P. K. *Surf. Interface Anal.* **2004**, *36*, 1314−1322.
(44) Liu, X. L.; Sun, K.; Wu, Z. Q.; Lu, J. H.; Song, B.; Tong, W. F.; Shi, X. J.; Chen, H. *Langmuir* **2012**, *28*, 9451−9459.
(45) Monticelli, F.; Toledano, M.; Osorio, R.; Ferrari, M. *Dent. Mater.* **2006**, *22*, 1024−1028.

(46) Kwak, D.; Wu, Y.; Horbett, T. A. *J. Biomed. Mater. Res.* **2005**, *74A*, 69−83.
(47) Shen, M.; Wagner, M. S.; Castner, D. G.; Ratner, B. D.; Horbett, T. A. *Langmuir* **2003**, *19*, 1692−1699.
(48) Eriksson, O.; Nygren, H. *J. Lab. Clin. Med.* **2001**, *137*, 296−302.
(49) Marcus, A. J. *Semin. Hematol.* **2000**, *31*, 261−269.
(50) Keselowsky, B. G.; Collard, D. M.; Garcia, A. J. *J. Biomed. Mater. Res.* **2003**, *66*, 247−259.